1   **Title:** Echolocation reverses information flow in a cortical vocalization network.

2

3   **Authors:** Francisco García-Rosales[1*], Luciana López-Jury[1], Eugenia Gonzalez-Palomares[1],

4   Johannes Wetekam[1], Yuranny Cabral-Calderín[2], Ava Kiai[1], Manfred Kössl[1], Julio C.

5   Hechavarría[1*].

6   **Affiliations:** [1] Institut für Zellbiologie und Neurowissenschaft, Goethe-Universität, 60438

7   Frankfurt/M., Germany. [2] Research Group Neural and Environmental Rhythms, Max Planck

8   Institute for Empirical Aesthetics, 60322 Frankfurt/M., Germany.

9   [*] *Corresponding authors.*

10

11   **Mailing address:**

12   * Francisco García-Rosales, Institut für Zellbiologie und Neurowissenschaft, Max-von-Laue-

13   Str. 13, 60438 Frankfurt/Main, Germany, Tel.: (+49) 69 / 798 42063. Email:

14   garciarosales@bio.uni-frankfurt.de

15   * Julio C. Hechavarria, Institut für Zellbiologie und Neurowissenschaft, Max-von-Laue-Str.

16   13, 60438 Frankfurt/Main, Germany, Tel.: (+49) 69 / 798 42062. Email:

17   hechavarria@bio.uni-frankfurt.de

18

Abstract

The mammalian frontal and auditory cortices are important for vocal behaviour. Here, using local field potential recordings, we demonstrate for the first time that the timing and spatial pattern of oscillations in the fronto-auditory cortical network of vocalizing bats (*Carollia perspicillata*) predict the purpose of vocalization: echolocation or communication. Transfer entropy analyses revealed predominantly top-down (frontal-to-auditory cortex) information flow during spontaneous activity and pre-vocal periods. The dynamics of information flow depended on the behavioural role of the vocalization and on the timing relative to vocal onset. Remarkably, we observed the emergence of predominantly bottom-up (auditory-to-frontal cortex) information transfer patterns specific echolocation production, leading to self-directed acoustic feedback. Electrical stimulation of frontal areas selectively enhanced responses to echolocation sounds in auditory cortex. These results reveal unique changes in information flow across sensory and frontal cortices, potentially driven by the purpose of the vocalization in a highly vocal mammalian model.

Introduction

Vocal production is a crucial behaviour that underlies the evolutionary success of various animal species. Several cortical and subcortical structures in the mammalian brain support vocalization [1], their activities related to vocal control [2, 3, 4], motor preparation [2, 5, 6], and feedback correction [7, 8]. However, the precise neural dynamics that underpin vocal production, and the nature of long-distance interactions in large-scale neural networks related to vocal utterance, remain poorly understood.

The connectivity patterns of the frontal cortex make it a major hub for cognitive control and behavioural coordination [9, 10, 11]. Frontal cortical areas are anatomically connected with structures directly involved in vocal production, such as the periaqueductal grey [12] and the dorsal striatum [13]. Experimental evidence demonstrates that the neural activity in frontal regions relates to vocalization [4, 14, 15, 16], correlating with the acoustic and behavioural properties of produced calls [14, 16]. Frontal regions are also anatomically and functionally connected with the auditory cortex (AC; [17, 18, 19, 20, 21, 22]), which exhibits suppression to self-produced sounds generated by body movements [23, 24, 25, 26] or vocalizations [27, 28, 29, 30]. This suppression is thought to be mediated by preparatory motor signals originating in the motor system (i.e. "corollary discharges" or "efference copies"; [31, 32, 33]). The attenuation of neural responses in AC during vocal production supports precise vocal control by means of feedback mechanisms [7, 8] in coordination with frontal cortical areas [34, 35, 36, 37]. Although current evidence shows that fronto-auditory circuits are essential for the accurate control of vocalization, neural interactions in these networks remain obscure.

In this study, we addressed the neural mechanisms of vocal production in the fronto-auditory system of a highly vocal mammal: the bat *Carollia perspicillata* [38, 39, 40, 41]. Bats constitute an excellent model to study the underpinnings of vocalization because they rely heavily on vocal behaviour for communication and navigation (i.e. echolocation). Communication and echolocation utterances are vocalized for very different behavioural purposes, and typically differ markedly in their spectrotemporal design [40]. The production of these calls is distinctly controlled at the level of the brainstem [42], possibly mediated by frontal cortical circuits involving regions such as the anterior cingulate cortex [43] and the frontal-auditory field (FAF; [16]).

Vocalization circuits were studied by measuring local-field potential (LFP; [44]) oscillations simultaneously in frontal and auditory cortex regions of vocalizing bats. In frontal and

3

65 sensory cortices, LFPs are involved in cognitive processes, sensory computations, and

66 interareal communication via phase coherence [17, 45, 46, 47, 48, 49]. In the FAF, a richly connected

67 auditory region of the bat frontal cortex [20, 50], LFP activity predicts vocal output and

68 synchronizes differentially with dorso-striatal oscillations according to vocalization type [16].

69 Oscillations in the bat frontal cortex synchronize across socially interacting bats [51], and seem

70 to be involved in the cognitive aspects of social exchange [52]. The roles of auditory cortical

71 oscillatory activity in vocal production are less clear, although human studies suggest that

72 oscillations mediate synchronization with frontal and motor areas for feedback control [35, 53, 54].

73 However, the precise dynamics of information exchange in the fronto-auditory circuit during

74 vocalization are unknown.

75 The goal of this study was to unravel the nature of information exchange in the bat's FAF-AC

76 network, and to understand whether information between these structures flows in accordance

77 with the canonical roles of the frontal cortex for vocal coordination, and of the AC for

78 feedback control. We further aimed to address whether the distinct behavioural contexts of

79 echolocation and communication affect the dynamics of information transfer in the fronto-

80 auditory circuit. We found complex causal interactions (within a transfer entropy framework)

81 between frontal and auditory cortices during spontaneous activity and periods of vocal

82 production. Directed connectivity in the FAF-AC network varied dynamically according to

83 whether animals produced communication or echolocation calls, and to the timing relative to

84 vocal onset. For echolocation the changes were drastic, resulting in a reversal of information

85 flow from pre-vocal to post-vocal periods. Altogether, our data suggest that dynamic

86 information transfer patterns in large-scale networks involved in vocal production, such as the

87 FAF-AC circuit, are shaped by the behavioural consequences of produced calls.

88 **Results**

89 Neural activity was studied in the FAF and AC of *C. perspicillata* bats (3 males) while

90 animals produced self-initiated vocalizations. From a total of 12494 detected vocalizations,

91 138 echolocation and 734 non-specific communication calls were preceded by a period of

92 silence lasting at least 500 ms and were therefore considered for subsequent analyses.

93 Representative echolocation and communication vocalizations are shown in **Fig. 1a**. Overall,

94 the two types of vocalizations did not differ significantly in terms of call length (Wilcoxon

95 rank sum test, p = 0.78; **Fig. 1b**), although call length distributions differed significantly (2-

96 sample Kolmogorov-Smirnov test, p = 7.93×10^{-7}). There were clear differences in the power

97   spectra of echolocation and communication calls (**Fig. 1c**, left), such that peak frequencies of

98   echolocation utterances were significantly higher than their communication counterparts

99   (Wilcoxon rank sum test, p = 2.24x10^{-66}; **Fig. 1c**, right). These differences are consistent with

100   the structure of echolocation and communication sounds in bats (*C. perspicillata*) described in

101   previous studies {Knornschild, 2014 #245}{Porter, 1979 #374}.

Oscillations in frontal and auditory cortices predict vocalization type

103   **Figure 1d** illustrates electrophysiological activity recorded simultaneously from FAF and AC

104   at various cortical depths, as the echolocation and communication vocalizations shown in **Fig.**

105   **1a** were produced (see location of recording sites in **Fig. S1**). Single-trial LFP traces revealed

106   conspicuous pre-vocal oscillatory activity in low and high-frequencies, more pronounced in

107   frontal regions, and strongest when animals produced echolocation pulses. Power spectral

108   densities (PSD) obtained from pre-vocal LFP segments (i.e. -500 to 0 ms relative to vocal

109   onset; **Fig. 1f**) indicated low- and high-frequency power increases (relative to a no-

110   vocalization baseline, or "no-voc") associated with vocal production, particularly in FAF and

111   for electrodes located at depths > 100 μm (**Fig. 1e** illustrates this at 300 μm; black arrows).

112   Differences in AC across types of vocal outputs were less pronounced and appeared limited to

113   low LFP frequencies (grey arrows in **Fig. 1e**). These pre-vocal spectral patterns were analysed

114   using canonical LFP frequency bands, namely: delta (δ), 1-4 Hz; theta (θ), 4-8 Hz; alpha (α),

115   8-12 Hz; low beta (β_1), 12-20 Hz; high beta (β_2), 20-30 Hz; and three sub-bands of gamma

116   (γ): γ_1 (30-60 Hz), γ_2 (60-120 Hz), and γ_3 (120-200 Hz). Pre-vocal LFP power in each band

117   normalized to no-voc periods on a trial-by-trial basis.

118   There were significant power changes between no-voc and pre-vocal periods across frequency

119   bands (**Fig. 1f**, **S2**). Notably, the power increase in low- (δ-α) and high-frequency (γ_2) LFP

120   bands of the FAF was different when animals produced echolocation and communication

121   vocalizations, with the highest increase in the pre-vocal echolocation case. The opposite

122   pattern was observed in the AC, where differences between ensuing vocalization types were

123   most prominent in β_1 (but not δ-α or γ) frequencies, and were explained by higher pre-vocal

124   power increase for communication than for echolocation vocalizations (**Fig. 1f**).

125   We addressed whether pre-vocal LFP power in frontal and auditory cortices was a significant

126   predictor of ensuing call type. To this effect, generalized linear models (GLMs) were fit using

127   echolocation and communication pre-vocal power changes as predictors, for all channels (in

128   both structures) and frequency bands. A summary of these models is given in **Fig. 1g** (see

5

129   outcomes of two representative GLMs illustrated in **Fig. S2**). Low- and high-frequency power

130   increase (mostly in the δ-α and γ_2 bands) in FAF predicted whether animals produced

131   echolocation or communication calls, typically with moderate effect sizes ($p < 0.05$; $R^2m >=$

132   0.1), highest in middle-to-deep electrodes (i.e. depths > 300 μm; **Fig 1g**, left). In the AC, pre-

133   vocal power predicted ensuing call type mostly in the α-β bands of the spectrum, although

134   more strongly in β_1 frequencies. Moderate effect sizes were also observed ($p < 0.05$; $R^2m >=$

135   0.1). Overall, pre-vocal oscillatory power significantly predicted ensuing call type in frontal

136   and auditory cortices with complementary frequency specificity and functionally opposite

137   effects.

138   We evaluated whether differences in the spectral dynamics of pre-vocal LFPs could be

139   explained by differences in the frequency content of echolocation and communication

140   utterances. To that end, communication calls were separated into two groups: high-frequency

141   and low-frequency communication (HF- and LF-communication, respectively). The spectral

142   content of pre-vocal LFPs predicted ensuing call type, even when HF-communication calls

143   were pitched against echolocation utterances ($p < 0.05$; $R^2m >= 0.1$; **Fig. S3**). Additionally,

144   pre-vocal spectral differences were considerably less noticeable when comparing HF- vs. LF-

145   communication vocalizations, with even significant models ($p < 0.05$) performing poorly in

146   FAF and AC ($R^2m < 0.1$; **Fig. S3b, d**). Thus, pre-vocal spectral differences are not fully

147   accounted for by differences in the spectral content of echolocation and communication calls.

148   <u>Directed connectivity in the FAF-AC circuit related to vocal production</u>

149   Oscillations in FAF and AC predict ensuing vocal output with functionally opposite patterns,

150   but how rhythms in this network interact during vocal production remains unknown. In

151   previous work, we reported low-frequency (1-12 Hz) phase coherence in the FAF-AC circuit

152   during spontaneous activity, with emergence of γ-band (> 25 Hz) coherence at the onset of

153   external acoustic stimulation [17]. To study FAF-AC oscillatory dynamics during vocal

154   production, we looked beyond phase correlations and examined causal interactions (within a

155   transfer entropy framework) in the fronto-auditory circuit. Causal interactions were quantified

156   using directed phase transfer entropy (dPTE), a metric that measures the degree of preferential

157   information transfer between signals based on phase time series [55, 56]. dPTE calculations were

158   performed across vocal conditions for all channel pairs, and for frequency bands which most

159   strongly predicted vocalization type: δ, θ, α, β_1, and γ_2.

160   Average dPTE connectivity matrices across conditions (echolocation and communication pre-

161   and post-vocal periods, and no-voc segments) are illustrated in **Fig. S4**. dPTE matrices were

162   used as adjacency matrices for directed graphs, which characterized patterns of directional

163   information flow in the FAF-AC network (**Fig. 2**). In each graph, nodes represent adjacent

164   channels pooled according to cortical depth and layer distribution in AC (where layer borders

165   are well-defined anatomically; **Fig. S1**): superficial (*sup*), channels 1-4 (0-150 μm); top-

166   middle (*mid1*), channels 5-8 (200-350 μm); bottom-middle (*mid2*), channels 9-12 (400-550

167   μm); and *deep*, channels 13-16 (600-750 μm). Directed edges were weighted according to a

168   directionality index (DI), obtained from normalizing dPTE values to 0.5 (dPTE = 0.5

169   indicates no preferred direction of information transfer). Only edges with significant DI

170   values, based on bootstrapping, are shown.

171   Upon inspection of the connectivity graphs, we noticed general patterns that entailed strong

172   top-down preferential information transfer (i.e. in the FAF → AC direction) during

173   spontaneous activity, pre-vocal periods irrespective of vocalization type, and post-vocal

174   communication periods (**Fig. 2**). Top-down information flow (blue arrows in the figure) was

175   strongest for δ, θ, and γ_2 frequencies, although also ocurred sparsely in α and β_1 bands with

176   patterns that depended on ensuing call type. Within FAF and during pre-vocal echolocation

177   periods, information flowed predominantly from deep to superficial layers in δ and β_1

178   frequencies (**Fig. 2b**), and in the opposite direction for α-LFPs, also during no-voc periods

179   (**Fig. 2a**, **b**). Within AC, information flowed in the superficial to deep direction during no-voc

180   and pre-vocal communication periods in γ_2 frequencies.

181   To our surprise, a predominance of bottom-up information flow (i.e. AC → FAF direction)

182   appeared to be specific to post-vocal echolocation periods in the δ and β_1 bands, although

183   bottom-up information transfer did occur in α frequencies during post-vocal communication

184   epochs (**Fig. 2c**). Note that, for echolocation, there was strong to-down information transfer

185   before vocalization onset, particularly in the δ-band (cf. **Fig. 2c** with **Fig. 2b**, top). These

186   results hint toward a pre- to post-vocal reversal of information flow in the FAF-AC network

187   during echolocation, evident in low frequencies of the LFP. Considering within-structure

188   information transfer, patterns were diverse in FAF, consisting of information exchange in the

189   deep-to-superficial (bands: δ, echolocation and communication; α, communication; and β_1,

190   both) and the superficial-to-deep (α-band, for echolocation) directions. Within AC,

191   predominant information flow occurred both in the superficial-to-deep (δ-band, echolocation)

7

192 and in the deep-to-superficial directions (bands: θ, echolocation; α, echolocation and

193 communication; β_1, echolocation, γ_2, communication) as well.

194 Taken together, the data in **Fig. 2** illustrate rich patterns of information exchange within and

195 between frontal and auditory cortices. Information transfer patterns depended on whether a

196 vocalization was produced and on its type, either considering within-structure connectivity, or

197 information transfer across regions. Differences in the information flow dynamics of the

198 fronto-auditory circuit, across vocal conditions and call-types, are depicted in **Figures S5** and

199 **S6**, and quantified in detail in the supplementary results.

200 <u>Information flow in the fronto-auditory circuit reverses for echolocation production</u>

201 The contrasts between pre- and post-vocal periods for echolocation (**Fig. 2b**, **c**) suggest that

202 the preferred directionality of information flow reverses when animals echolocate.

203 Differences in the direction of information transfer between pre-vocal and post-vocal

204 activities were addressed by statistically comparing connectivity graphs associated to each

205 case (**Fig. 3**). Paired statistics were performed for these comparisons (Wilcoxon singed-rank

206 tests, significance when $p < 10^{-4}$; see Methods); edges, representing significant differences in

207 dPTE, were only shown for large effect sizes ($|d| > 0.8$). As expected from the data depicted in

208 **Figure 2**, echolocation-related FAF → AC preferred information flow was significantly

209 higher during pre-vocal than post-vocal periods in the δ and θ bands (**Fig. 3a**, top). In γ_2

210 frequencies, the effect was the opposite: FAF → AC directionality was highest during post-

211 vocal periods than during pre-vocal ones. Remarkably, AC → FAF preferred directionality of

212 information flow was significantly stronger during post-vocal periods in δ and β_1 frequency

213 bands (**Fig. 3a**, top). Within FAF, differences in preferred information flow occurred in

214 frequency bands δ, α, and β_1. Within AC, differences in dPTE occurred mostly in α and β_1

215 bands (**Fig. 3a**, top). Information flow was strongest in the deep-to-superficial direction

216 during post-vocal periods, and in superficial-to-deep directions during pre-vocal periods. In

217 the case of communication call production (**Fig. 3b**, top), differences in dPTE occurred only

218 in the δ and θ bands. Values were significantly higher (with large effect sizes) in the FAF →

219 AC direction during pre-vocal periods.

220 Changes in directional information transfer in the FAF-AC network were quantified by

221 calculating the net information outflow (DI_{net}) from each area. The DI_{net} represents the sum of

222 DI values obtained from outgoing connections per region (e.g. all edges in FAF related to

223 FAF → AC connections, representing the net strength of preferential information flow in the

224   fronto-auditory direction). DI_{net} values were used to statistically compare pre- and post-vocal

225   periods in terms of information transfer from one cortical area to another. Considering this

226   metric, significant differences (FDR-corrected Wilcoxon singed-rank tests, $p_{corr} < 0.05$) with

227   large effect sizes ($|d| > 0.8$) occurred mostly for low and intermediate frequency bands (i.e. δ

228   and β_1) of the LFP. Specifically, for the pre-vocal vs. post-vocal echolocation condition (**Fig.**

229   **3a**, bottom), the information outflow from FAF was significantly higher in the δ band during

230   pre-vocal periods related to echolocation call production ($p_{corr} = 1.63 \times 10^{-82}$, $d = 3.44$).

231   Notably, the net information outflow from AC was significantly higher when considering

232   post-vocal periods than pre-vocal ones ($p_{corr} = 3.27 \times 10^{-64}$, $d = -1.5$). In the β_1 frequency range,

233   there were no significant differences with large effect sizes between pre-vocal and post-vocal

234   net information outflow from the FAF. However, DI_{net} values from AC were significantly

235   higher during post-vocal periods ($p_{corr} = 3.71 \times 10^{-36}$, $d = -0.88$). Pre-vocal vs. post-vocal

236   comparisons of DI_{net} values from FAF and AC related to communication calls revealed

237   significant differences with large effect sizes only for δ frequencies in FAF (**Fig. 3b**, bottom;

238   DI_{net} higher for pre-vocal periods: $p_{corr} = 1.63 \times 10^{-82}$, $d = 1.39$).

239   The passive listening of echolocation-like or communication sounds did not account for the

240   data above (**Fig. S7-9**), suggesting that mere feedback from the calls was not sufficient to

241   explain echolocation-related, δ-band information flow reversal in the network. Likewise, the

242   production of HF-communication sounds did not account for the patterns observed during

243   echolocation (**Fig. S10**), indicating that the information transfer dynamics for echolocation are

244   not fully explained by the frequency content of the vocalizations themselves. Altogether,

245   these results unveil dynamic changes of predominant connectivity patterns in the FAF-AC

246   network from pre- to post-vocal periods, exhibiting frequency specificity and particularly

247   associated with echolocation production.

248   <u>Electrical stimulation of the FAF enhances auditory cortical responses</u>

249   The data thus far indicate strong top-down modulation in the FAF-AC network, which can

250   nevertheless be significantly altered when animals produce echolocation sounds. However,

251   the dPTE analyses cannot rigorously establish whether FAF activity indeed modulates AC

252   responses. To examine this question, we conducted perturbation experiments of the FAF to

253   evaluate whether manipulations in this region affect auditory cortical responses to external

254   sounds.

255   The FAF was stimulated electrically with biphasic pulse trains (6 pulses/train; pulse interval:

256   500 ms) while simultaneously recording from the AC (n = 20 penetrations; **Fig. 4a**). Electrical

257   stimulation of FAF did not produce detectable artefacts or LFP power changes in AC (**Figs.**

258   **4c** and **S11**), nor did it elicit vocalization production (**Fig. S12**), potentially due to weaker

259   stimulation as compared to previous work with measurable behavioural outputs [43, 57]. Acoustic

260   stimuli were presented after the train (either a distress -a type of communication sound- or an

261   echolocation call; see **Fig. S7b**, and **Fig. 4b**) at different delays. Response strengths in AC to

262   sounds after FAF electrical stimulation ("Estim" condition) were compared to response

263   strengths related to the same sounds, but presented without prior electrical stimulation ("no-

264   Estim" condition). Representative responses to distress and echolocation calls for both

265   conditions and for a delay of 135 ms (in the Estim case) are depicted in **Fig. 4d**.

266   We observed differences between the ERP energy measured in Estim and no-Estim conditions

267   (red and blue, respectively), more evidently when considering AC responses to echolocation

268   sounds (**Fig. 4d**). These differences occurred consistently at a population level. **Figure 4e**

269   depicts response strengths for all AC depths across recordings, related to a distress syllable

270   presented with a delay of 135 ms (in the Estim case; red traces). Response strengths from the

271   no-Estim case are shown for one example iteration out of 500 conducted for comparisons (see

272   Methods). A trend was present, wherein responses in the Estim condition were stronger than

273   those in the no-Estim condition, although without statistically significant differences (**Fig. 5f**;

274   FDR-corrected Wilcoxon signed-rank tests, significance if $p_{corr} < 0.05$). Overall, when

275   acoustic stimulation was done with a distress syllable, significant differences between Estim

276   and no-Estim occurred in ~40 % of out 500 iterations in total. Such differences were

277   concentrated mostly in middle-to-deep layers (depths > 300 μm) with small to medium values

278   of Cliff's delta ([58]; **Fig. 4i**, **j**, *left*).

279   In terms of AC responses to echolocation sounds (**Fig. 4g**), differences between Estim and no-

280   Estim conditions appeared most prominent in superficial-to-middle layers (depths 50 – 350

281   μm). Responses were significantly stronger in the Estim condition than in the no-Estim

282   condition at depths of 50 – 300 μm (**Fig. 4h**; $p_{corr} < 0.05$), in particular for a sound-delay of

283   135 ms. Significant differences between Estim and no-Estim conditions were very reliable,

284   observed in up to 90.6 % of the iterations for a delay of 135 ms and a cortical depth of 150

285   μm (**Fig. 4i**, *right*). At depths ranging 50-350 μm, for the same delay, reliability was larger

286   than 70 %, with medium effect sizes (**Fig. 4j**, *right*). These data indicate that electrical

287   stimulation on the FAF enhances response strength in the AC, with particularly high

288   reliability when the animals listen to echolocation sounds.

Discussion

289

290   In this study, we addressed the dynamics of information exchange between frontal and

291   auditory cortices of vocalizing bats (summarized in **Fig. 5**). Consistent with previous reports [4,

292   14, 16, 35, 46, 59], we show that neural activity in the frontal cortex predicts vocal outputs. Taken

293   together, the data from this and previous work suggest that oscillations in frontal regions may

294   be instrumental for vocal production. From our perspective, the above is further supported by

295   call-type specific, pre-vocal LFP spectral dynamics and information transfer patterns in the

296   FAF-AC network. The relationship between oscillations and vocal production remains,

297   nevertheless, correlational: our results do not allow to rigorously assert a causal role of LFPs

298   for the initiation or planning of vocal outputs.

299   Neural activity in the AC also relates to vocalization [27], but the involvement of auditory

300   cortical oscillations in vocal production is still to be fully understood. Our results indicate that

301   pre-vocal LFPs in AC, as previously reported with single-unit spiking [27, 29, 30], relate to vocal

302   initiation. We show, for the first time to our knowledge, that pre-vocal oscillatory patterns in

303   AC are call-type specific and, remarkably, complementary to those observed in frontal cortex

304   in frequency and effect (**Fig. 1**). These patterns may be explained by our current

305   understanding of the roles of AC for vocal production. Neuronal activity in the AC is

306   predominantly suppressed during vocalization, with inhibition occurring hundreds of

307   milliseconds prior to call onset [8, 27, 28, 60]. Vocalization-related inhibition is mediated by motor

308   control regions, which send a copy of the motor command to the AC as "corollary discharge"

309   or "efferent copy" signals [33, 61]. These signals, respectively, have either a general suppressive

310   effect, or carry specific information about the produced sound which potentially facilitates

311   feedback processing [32]. Thus, pre-vocal, call-type unspecific power changes in low

312   frequencies could reflect general inhibitory mechanisms in AC consistent with corollary

313   discharges from higher order structures. Directed connectivity analyses support the notion of

314   top-down (FAF → AC) control of pre-vocal low-frequency activity (**Fig. 2**). In contrast, pre-

315   vocal β-band LFPs might constitute oscillatory correlates of efference copies, given the

316   observed call-type specificity. Because FAF → AC causal influences did not equally extend

317   to the β frequencies, pre-vocal β activity in AC might be influenced instead by specialized

318   regions such as the premotor cortex, providing a more specific copy of the motor commands

319   required for vocalization. Channels for motor-auditory communication (see [62, 63]) could in fact

320   operate over β frequencies [53, 64, 65].

321   Differences in spectral patters cannot be solely explained by the distinct frequency content of

322   echolocation and communication calls (**Fig. S3**). However, considering that orofacial

323   movement in primates [15, 66] and vocalization-specific movements in bats [50] are associated to

324   neural activity in frontal areas, distinct pre-vocal motor related activity for echolocation or

325   communication calling is a plausible explanation for our results. Microstimulation of *C.*

326   *perpsicillata*'s FAF can result in motor effects such as pinna and nose-leaf movements, as

327   well as vocalizations (including echolocation-like calls; [50]). These movements also occur

328   naturally before spontaneous vocalization [50], suggesting that the FAF may be involved in the

329   motor aspect of vocal production. Nevertheless, vocalization-specific neural populations in

330   primates coexist with those related to orofacial movements [67]. Therefore, the vocal-motor

331   explanation does not necessarily entail that the FAF fails to participate in other forms of vocal

332   preparation beyond the orchestration of motor programs.

333   In terms of a cortical network for vocalization, the FAF and AC are engaged in rich

334   information transfer dynamics with functional relationships to vocalization. Moreover,

335   interactions extend to periods of vocal quiescence, when information flows top-down (FAF →

336   AC) in low (δ-α) and high (γ$_2$) frequencies. Low-frequency top-down influences from higher-

337   order structures (like the FAF) modulate neuronal activity in sensory cortices according to

338   cognitive variables such as attention, also during spontaneous activity [55, 68, 69]. However,

339   whether and how attentional processes exploit the nature of neural connections in the FAF-

340   AC circuit remains thus far unknown. Our data resonate with the hypothesis of top-down

341   modulation of oscillatory activity in AC, and suggest a strict control of higher-order structures

342   over sensory areas reflected in concurrent LFP activity across regions. Such strong top-down

343   control is supported by the fact that FAF microstimulation enhances auditory cortical

344   responses to sounds (**Fig. 4**).

345   Vocalization-specific changes in power may affect causality estimations, e.g. by creating

346   confounding differences between the vocal conditions studied. However, the dPTE is a

347   causality estimate that shows robustness to the influence of power, noise, and other variables.

348   In our dataset, the pre-vocal δ-band power increase within each region when animals

349   produced echolocation (call-type specific in FAF, unspecific in AC) was nonetheless

350   accompanied by a decrease of interareal dPTE values. In addition, a δ-band power increase of

12

351 communication pre-vocal LFPs relative to baseline (**Figs. 1**, **S1**) did not result in significant

352 differences of dPTE values during pre-vocal and spontaneous periods. Thus, changes in

353 causality did not necessarily follow changes in power, as has been reported in previous work

354 {Hillebrand, 2016 #559}.

355 Based on dPTE values associated with spontaneous and pre-vocal activities (**Fig. 2** and **S5**), it

356 appears that as animals prepare the production of an echolocation call, the FAF gradually

357 relinquishes control over the AC in the low-frequency (δ) channel. That is, the top-down

358 control wanes during echolocation pre-vocal periods in δ LFPs. The weakening of preferred

359 top-down information transfer could be taken as a preamble of emerging bottom-up

360 information flow in δ frequencies after an echolocation call is emitted (**Fig. 3**). This fails to

361 happen in the communication case. Echolocation, the predominant strategy for navigation, is

362 essential for bats. After vocalizing an echolocation pulse, the bat auditory system must be

363 ready to process incoming echoes and use them to construct a representation of surrounding

364 objects [70], potentially involving higher order structures. The observed switch from top-down

365 to bottom-up processing when animals find themselves in echolocation mode could represent

366 the readiness of the bat's auditory machinery for the aforementioned task. Concretely, our

367 data suggest that the former may occur over a continuum encompassing a gradual release of

368 the AC from top-down influences (i.e. from the FAF), which opens the way for auditory-

369 frontal information transfer supporting the processing and integration of incoming echoes. A

370 reversal in information transfer is also visible (albeit weaker and in a different LFP frequency

371 band) during the production of high frequency communication sounds (**Fig. S10**). This result

372 could hint towards smooth transition in the way the FAF-AC network operates, which finds

373 its two extremes in echolocation and low-frequency communication call production.

374 In all, processing feedback information directly related to navigation appears to have a larger

375 weight in the bottom-up processing of acoustic cues resulting from a self-generated sound.

376 Echolocation pulses are produced to generate echoes that must be listened to. Communication

377 calls are often targeted to an audience as means of transmitting internal behavioural

378 information (e.g. distress, aggressive mood, etc.), not aimed at the emitter itself. For the

379 emitter, in such scenario, feedback processing mostly contributes to the adjustment of vocal

380 parameters such as loudness or pitch [7, 71, 72]. Since in this study animals vocalized without an

381 audience (i.e. they were isolated in the recording chamber), further research could elucidate

382 whether the presence of conspecifics increases bottom-up information transfer when

383 vocalizing communication calls, as animals could expect a response.

13

384   The reversal of information flow reported in the δ-band when animals echolocate cannot be

385   solely attributed to passively hearing feedback from their own utterances (**Fig. S7-10**): active

386   vocalization seems to be necessary to trigger bottom-up information transfer in the FAF-AC

387   circuit. The current data, together with the fact that passive listening fails to significantly alter

388   low-frequency coherence in the FAF-AC network [17], indicate that passive listening alone is

389   not sufficient to significantly alter the dynamics of communication between FAF and AC.

390   Likewise, information flow dynamics associated to echolocation calls could not be attributed

391   to their high frequency content alone, since qualitatively similar differences between

392   echolocation and communication calls were observed when considering only HF-

393   communication utterances, particularly for δ-LFPs (**Fig. S10**). Echolocation, therefore,

394   triggers unique patterns of information flow reversal in the fronto-auditory network of *C.*

395   *perspicillata*. Our data indicates that the connectivity in this circuit is shaped by the

396   behavioural implications of the calls produced.

397   The transfer entropy analyses discussed above indicate that the frontal cortex exerts top-down

398   modulation over its auditory cortical counterpart, particularly during spontaneous activity

399   (**Fig. 2**). Consistent with the top-down modulation perspective, electrical perturbation of the

400   FAF enhanced the strength of responses in AC, echoing known effects of frontal stimulation

401   in other mammals [21]. Given that FAF manipulation most reliably altered responses to

402   echolocation sounds (**Fig. 4**), and that the production of echolocation pulses reverses

403   information flow in the fronto-auditory circuit, the data suggest that dynamic interactions in

404   the bat's FAF-AC network favour echolocation behaviour.

405   **Methods**

406   <u>Animal preparation and surgical procedures</u>

407   The study was conducted on five awake *Carollia perspicillata* bats (one female).

408   Experimental procedures were in compliance with European regulations for animal

409   experimentation and were approved by the Regierungspräsidium Darmstad (experimental

410   permit #FU-1126 and FR-2007). Bats were obtained from a colony at the Goethe University,

411   Frankfurt. Animals used for experiments were kept isolated from the main colony.

412   Prior to surgical procedures, bats were anaesthetized with a mixture of ketamine (10

413   mg*kg−1, Ketavet, Pfizer) and xylazine (38 mg*kg−1, Rompun, Bayer). For surgery and for

414   any subsequent handling of the wounds, a local anaesthetic (ropivacaine hydrochloride, 2

415   mg/ml, Fresenius Kabi, Germany) was applied subcutaneously around the scalp area. A

416   rostro-caudal midline incision was cut, after which muscle and skin tissues were carefully

417   removed in order to expose the skull. A metal rod (ca. 1 cm length, 0.1 cm diameter) was

418   attached to the bone to guarantee head fixation during electrophysiological recordings. The

419   FAF and AC were located by means of well-described landmarks, including the sulcus

420   anterior and prominent blood vessel patterns (see [17, 50, 73]). The cortical surface in these

421   regions was exposed by cutting small holes (ca. 1 mm^2) with the aid of a scalpel blade on the

422   first day of recordings. In the AC, recordings were made mostly in the high frequency fields

423   [17, 50, 73])

424   After surgery, animals were given no less than two days of rest before the onset of

425   experiments. No experiments on a single animal lasted longer than 4 h per day. Water was

426   given to the bats every 1-1.5 h periods, and experiments were halted for the day if the animal

427   showed any sign of discomfort (e.g. excessive movement). Bats were allowed to rest a full

428   day between consecutive experimental sessions.

429   Electrophysiological and acoustic recordings

430   Electrophysiology was performed chronically in fully awake animals, inside a sound-proofed

431   and electrically isolated chamber. Inside the chamber, bats were placed on a custom-made

432   holder which was kept at a constant temperature of 30 °C by means of a heating blanket

433   (Harvard, Homeothermic blanket control unit). Electrophysiological data were acquired from

434   FAF and AC on the left hemisphere, using two 16-channel laminar electrodes (one per

435   structure; Model A1x16, NeuroNexus, MI; 50 μm channel spacing, impedance: 0.5-3 MW per

436   electrode). Probes were carefully inserted into the brain perpendicular to the cortical surface,

437   and lowered with piezo manipulators (one per probe; PM-101, Science 455 products GmbH,

438   Hofheim, Germany) until the top channel was barely visible above the surface of the tissue.

439   The placing and properties of the probes allowed us to record simultaneously at depths

440   ranging from 0-750 μm, spanning all six cortical layers (see [74]). Probes were connected to a

441   micro-preamplifier (MPA 16, Multichannel Systems, MCS GmbH, Reutlingen, Germany),

442   and acquisition was done with a single, 32-channel portable system with integrated

443   digitization (sampling frequency, 20 kHz; precision, 16 bits) and amplification steps (Multi

444   Channel Systems MCS GmbH, model ME32 System, Germany). Acquisition was online-

445   monitored and stored in a computer using the MC_Rack_Software (Multi Channel Systems

446   MCS GmbH, Reutlingen, Germany; version 4.6.2).

447   Vocal outputs were recorded by means of a microphone (CMPA microphone, Avisoft

448   Bioacustics, Glienicke, Germany) located 10 cm in front of the animal. Recordings were

449   performed with a sampling rate of 250 kHz and a precision of 16 bits. Vocalizations were

450   amplified (gain = 0.5, Avisoft UltraSoundGate 116Hm mobile recording interface system,

451   Glienicke, Germany) and then stored in the same PC used for electrophysiology.

452   Electrophysiological and acoustic data were aligned using two triggers, an acoustic one (5

453   kHz tone, 10 ms long) presented with a speaker located inside of the chamber (NeoCD 1.0

454   Ribbon Tweeter; Fountek Electronics), and a TTL pulse sent to the recording system for

455   electrophysiology (see above). Note that the onsets of the tones were in synchrony with the

456   TTL pulses registered by the acquisition system for electrophysiology.

457   <u>Acoustic stimulation</u>

458   Two acoustic stimuli were used to evaluate transfer entropy patterns during passive listening.

459   One of them, the high-frequency frequency modulated sound (HF-FM; 2 ms long; downward

460   frequency sweep from 80-50 kHz), mimicked the spectrotemporal structure of echolocation

461   pulses; the other, consisted of a distress syllable (distress, 3.8 ms long) typical of *C.*

462   *perspicillata*'s vocal repertoire. The latter stimulus was embedded in a sequence in which the

463   syllable was presented every 500 ms for 2 seconds (2 Hz rate); other sequences with faster

464   rates were also presented to the animal, but were not considered for this study. Only the first

465   syllable of the 2 Hz sequence was used for analyses. Stimuli for determining frequency tuning

466   consisted of short (10 ms) pure tones at various frequencies (5-90 kHz, in steps of 5 kHz) and

467   levels (15-75 dB SPL, steps of 15 dB). Since the HF-FM and the distress sounds were

468   presented at 70 dB SPL (rms), we focused on the frequency tuning curved obtained with pure

469   tone stimuli presented at 75 dB SPL.

470   The setup for stimulation has been described in previous studies (see [17]). In short, sounds were

471   digital-to-analog converted using a sound card (M2Tech Hi-face DAC, 384 kHz, 32 bit),

472   amplified (Rotel power amplifier, model RB-1050), and presented through a speaker

473   (description above) inside of the chamber. The speaker was located 12 cm away from the bat's

474   right ear, contralateral to the cerebral hemisphere on which electrophysiological recordings

475   were made. Prior to stimulation, sounds were downsampled to 192 kHz and low-pass filtered

476   (80 kHz cut-off) Sound presentation was controlled with custom written Matlab softwares

477   (version 8.6.0.267246 (R2015b), MathWorks, Natick, MA) from the recording computer.

478   Classification of vocal outputs

479   Two sessions of concurrent acoustic recordings (~10 min long) were made per paired

480   penetrations in FAF and AC. Vocalizations were automatically detected based on the acoustic

481   envelope of the recordings. The envelope was z-score normalized to a period of no

482   vocalization (no less than 10 s long), which was manually selected, per file, after visual

483   inspection. If a threshold of 5 standard deviations was crossed, a vocalization occurrence was

484   marked and its start and end times were saved. Given the stereotyped spectral properties of *C.*

485   *perspicillata*'s echolocation calls, a preliminary classification between echolocation and

486   communication utterances was done based on each call's peak frequency (a peak frequency >

487   50 kHz suggested an echolocation vocalization, whereas a peak frequency below 50 kHz

488   suggested a communication call). In addition, vocalizations were labelled as candidates for

489   subsequent analyses if there was a time of silence no shorter than 500 ms prior to call

490   production to ensure no acoustic contamination on the pre-vocal period that could affect LFP

491   measurements in FAF or AC. Finally, echolocation and communication candidate

492   vocalizations were individually and thoroughly examined via visual inspection to validate

493   their classification (echolocation or communication), the absence of acoustic contamination in

494   the 500 ms prior to vocal onset, and the correctness of their start and end time stamps.

495   According to the above, and out of a total of 12494 detected vocalizations, 138 echolocation

496   and 734 communication calls were then used in further analyses.

497   High-frequency communication calls (HF-communication) were selected according the

498   frequency component of the vocalizations. Specifically, an HF-communication call was a

499   communication utterance with more than 50 % of its power in the 50-100 kHz range. HF-

500   communication calls represented 21.12% of the communication calls used (155/734).

501   Extraction of LFP signals and power analyses

502   Data analyses were performed using custom-written scripts in MatLab (versions

503   9.5.0.1298439 (R2018b), and 9.10.0.1684407 (R2021a)), Python (version 2.6 or 3.6), and R

504   (RStudio version 1.3.1073). For extracting LFPs, the raw data were band-pass filtered (zero-

505   phase) between 0.1 and 300 Hz (4th order Butterworth filter; *filtfilt* function, MatLab), after

506   which the signals were downsampled to 1 kHz.

507   All LFP spectral analyses were done using the Chronux toolbox [75]. Pre-vocal power was

508   calculated with LFP segments spanning -500-0 ms relative to vocal onset, using a TW of 2,

17

509   and 3 tapers. No-vocalization baseline periods (*no-voc*) with a length of 500 ms were pseudo-

510   randomly selected and their power spectra calculated in order to obtain baseline power values

511   for spontaneous activity. The total number of *no-voc* periods matched the total number of

512   vocalizations (n = 872), in a way that the number of selected *no-voc* periods per recording file

513   matched the number of vocalizations found in that particular file. The power of individual

514   frequency bands (i.e. δ, 1-4 Hz; θ, 4-8 Hz; α, 8-12 Hz; β_1, 12-20 Hz; β_2, 20-30 Hz; γ_1, 30-60

515   Hz; γ_2, 60-120 Hz; γ_3, 120-200 Hz) was calculated by integration of the power spectral density

516   accordingly for each case. Finally, the increase of pre-vocal power relative to the baseline

517   periods was calculated as follows (per frequency band, on a call-by-call basis):

518   $$Relative\ power\ change = \frac{BP_{pre-voc} - BP_{no-voc}}{BP_{no-voc}} * 100 \qquad [1],$$

519   where $BP_{pre-voc}$ is the pre-vocal power (in the case of either an echolocation or communication

520   vocalization) of the given frequency band and a trial (i.e. a specific call), and BP_{no-voc} is the

521   baseline no-voc power associated to the same frequency band and trial.

522   <u>Generalized linear model for vocal output prediction</u>

523   To determine whether pre-vocal power change relative to baseline was able to predict the type

524   of ensuing vocal output, we used a GLM with a logistic link function (i.e. logistic regression).

525   The model analysis was done in Rstudio with the *lme4* package. In brief, logistic regression

526   was used to predict the probability of a binary outcome (0 or 1; communication or

527   echolocation, respectively) based on the pre-vocal power change as the predictor variable.

528   The probabilities are mapped by the inverse logit function (sigmoid):

529   $$\sigma(x) = \frac{1}{1+\exp(-x)} \qquad [2],$$

530   which restricts the model predictions to the interval [0, 1]. Because of these properties, a

531   logistic regression with GLMs is well suited to compare data (and thus, evaluate predictions

532   of ensuing vocal-output) on a single-trial basis [76].

533   To estimate the effect size of the fitted models, we used the marginal coefficient of

534   determination (R^2m) with the *MuMIn* pacakage. The R^2m coefficient quantifies the variance

535   in the dependent variable (echolocation vs. communication vocalization) explained by the

536   predictor variable (i.e. the relative pre-vocal power change). This value is dimensionless and

537   independent of sample size [76, 77], which makes it ideal to compare effect sizes of different

18

538   models (e.g. across channels and frequency bands, as in **Fig. 1g**). Effect sizes were considered

539   small when $R^2m < 0.1$, medium when $0.1 <= R^2m < 0.4$, and large when $R^2m >= 0.4$ [76].

540   <u>Directionality analyses</u>

541   Directional connectivity in the FAF-AC network was quantified with the directed phase

542   transfer entropy (dPTE; [55]), based on the phase transfer entropy (PTE) metric [78]. PTE is a

543   data-driven, non-parametric directionality index that relates closely to transfer entropy (TE;

544   [79]), but is based on the phase time-series of the signals under consideration (here, FAF and

545   AC field potentials). PTE is sensitive to information flow present in broad- and narrowband

546   signals, and is in a large degree robust to the effects of, for example, noise, linear mixing, and

547   sample size [78, 80].

548   In terms of TE, a signal X causally influences signal Y (both of them can be considered as

549   phase times series), if the uncertainty about the future of Y can be reduced from knowing both

550   the past of signal X and signal Y, as compared to knowing the past of signal Y alone.

551   Formally, the above can be expressed as follows:

552    $$TE_{xy} = \sum p(Y_{t+\delta}, Y_t, X_t)\log(\frac{p(Y_{t+\delta}|Y_t, X_t)}{p(Y_{t+\delta}|Y_t)}) \quad [4],$$

553   where δ represents the delay of the information transfer interaction, and TE_{xy} is the transfer

554   entropy between signals X and Y. The estimation of the probabilities for TE quantification

555   requires large computational times and the tuning of various parameters [55]. PTE, on the other

556   hand, converts the time series into a sequence of symbols (binned-phase time series, see

557   below), and is able to estimate TE on the phase series reducing significantly both processing

558   times and the necessity for parameter fitting [78].

559   Phase time series were obtained after filtering the LFP signals in a specific frequency band

560   (e.g. θ, 4-8 Hz) and Hilbert transforming the filtered data. To avoid edge artefacts, the full

561   ~10 minutes recordings were filtered and Hilbert transformed before chunking segments

562   related to individual trials (i.e. pre-voc: -500-0 ms relative to call onset, post-voc: 0-250 ms

563   relative to call onset, or no-voc baseline periods). According to the condition under

564   consideration (echolocation/communication and pre-voc/post-voc, or baseline periods), we

565   selected 50 trials pseudo-randomly and then concatenated them before quantifying directional

566   connectivity. This process was repeated 500 times and the distribution of dPTE values

567   obtained from each repetition used for further analyses. The former resulted in a distribution

568   of 500 dPTE connectivity matrices; the median value across these was used for constructing

569   connectivity graphs (see below).

570   Given the phase of the LFP signals, the PTE was calculated according to equation [4].

571   However, probabilities in this case were estimated by constructing histograms of binned

572   phases [78] instead of using the full, continuous time series. Following [81], the number of bins in

573   the histograms was set to:

574
$$3.49 * \mu\big(\sigma(\phi)\big) * N_s^{-\frac{1}{3}} \qquad [5],$$

575   where m and s represent the mean and standard deviation, respectively, f represents the phase

576   time series, and N_s denotes the number of samples.

577   The prediction delay d was set to $(N_s \ x \ N_{ch})/ N_{+-}$ [55], where N_s and N_{ch} are the number of

578   samples and channels ($N_{ch} = 32$), respectively. The value of N_{+-} corresponds to the number of

579   times the LFP phase changes sign across all channels and times.

580   The dPTE was calculated from the PTE as follows [55]:

581
$$dPTExy = \frac{PTExy}{PTExy+PTEyx} \qquad [6]$$

582   With values ranging between 0 and 1, dPTEs > 0.5 indicate information flow preferentially in

583   the $X \rightarrow Y$ direction, dPTE values below 0.5 indicate preferential information flow in the

584   opposite direction, and dPTE = 0.5 indicates no preferred direction of information flow. In

585   other words, dPTE is a metric of preferred directionality between two given signals. Note that

586   the dPTE analysis among a set of electrodes yields a directed connectivity matrix that can be

587   considered as an adjacency matrix of a directed graph (see below). All PTE and dPTE

588   calculations were done with the Brainstorm toolbox in MatLab [82].

589   Connectivity graphs

590   A graph-theoretic examination of the connectivity patterns was made by constructing directed

591   graphs based on the results obtained from the dPTE analyses (i.e. the median across the 500

592   repetitions; see above). For simplicity, channels in the FAF and AC within a range of 150 μm

593   were grouped as follows (in the FAF, as an example): FAF$_{top}$, channels 1-4 (0-150 μm);

594   FAF$_{mid1}$, channels 5-8 (200-350 μm); FAF$_{mid2}$, channels 9-12 (400-550 μm); FAF$_{bottom}$,

595   channels 13-16 (600-750 μm). A similar grouping was done for electrodes located in AC.

596   These channel groups were considered as the nodes of a directed graph. A directed edge *(u, v)*

597   between any two nodes then represents a preferential information flow from node *u* to node *v*.

598   The weight of the edge was taken as the median dPTE for the channel groups corresponding

599   to the nodes, according to the dPTE connectivity matrices. For instance, if the groups

600   considered were FAF_{top} and AC_{bottom}, then the weight between both nodes was the median of

601   the obtained dPTE values calculated from channels 1-4 in FAF towards channels 13-16 in

602   AC. The weight of an edge was quantified as a directionality index (DI):

603    $$DI = \frac{median(dPTE_{uv}) - 0.5}{0.5} * 100 \qquad [7],$$

604   which expresses, in percentage points, the strength of the preference of information flow in a

605   certain direction. Equation [6] is based on the fact that a dPTE of 0.5 corresponds to no

606   preferred direction of information flow [55].

607   To statistically validate the directionality shown in the graphs we used a bootstrapping

608   approach. Surrogate adjacency matrices were built for the same channel groups (top, mid1,

609   mid2 and bottom), but electrodes were randomly assigned to each group, independently of

610   their depths or cortical location. This randomization was done independently within each of

611   the 500 dPTE matrices obtained from the main connectivity analysis. Then, an adjacency

612   matrix was obtained from these surrogate data in the same way as described above (i.e. using

613   the median across 500 randomized dPTE matrices). Such a procedure was repeated 10,000

614   times, yielding an equal number of surrogate graphs. An edge in the original graph was kept if

615   the DI of that edge was at least 2.5 standard deviations higher than the mean of the surrogate

616   distribution obtained for that edge (i.e. higher than the 99.38% of the surrogate observations).

617   Edges that did not fulfil this criterion were labelled as non-significant and were therefore not

618   considered for any subsequent analyses.

619   Directionality analyses for passive listening conditions

620   dPTE values and connectivity graphs for passive listening conditions were quantified using

621   the same methodology described for the cases of active vocalization. Analyses based on

622   responses to acoustic stimulation were made on a trial-by-trial basis. Trials were randomly

623   selected 500 times across all penetrations, depending on whether responses to the HF-FM or

624   the distress sound were considered. We ensured that the number of trials chosen for each

625   penetration, in every randomization run, matched the number of vocalizations taken (in a HF-

626   FM/echolocation or distress/communication scheme) from that particular penetration. With

627   this we aimed to avoid possible biases in the comparisons across passive listening and active

628   vocalizations conditions.

629   <u>Electrical stimulation experiments</u>

630   The FAF was electrically stimulated by means of biphasic pulses lasting 410 μs (200 μs per

631   phase, with 10 a μs gap between them) and with an amplitude of 2 μA. Electric pulses were

632   delivered by inserting an A16 Neuronexus shank (same used for recordings) into the frontal

633   cortex, using the channels at depths of 350 and 450 μm as stimulating electrodes. These

634   channels were directly connected to the outputs of an A365 stimulus isolator (World Precision

635   Instruments, Friedberg, Germany). Pulse amplitude was selected based on values used in the

636   literature (e.g. [83, 84, 85]), and after empirically establishing that electrical artefacts were

637   undetectable in the AC online during recordings. Recordings in AC were conducted with a

638   second A16 shank (as described above); in the AC no electrical stimulation was delivered.

639   Precisely, the electrical and acoustic stimulation protocol was as follows. Six biphasic electric

640   pulses were delivered into FAF with inter-pulse intervals of 500 ms (2 Hz, within the δ-band

641   range). After the electrical pulse train, acoustic stimuli were presented to the bats at given

642   delays relative to the time last electrical pulse (10, 135, 260, 385, 510, 635, 760 and 885 ms;

643   "Estim" condition). Delays were consistently with sampling four different phases per

644   electrical stimulation cycle (period is considered as the inter-pulse interval), for a total of 2

645   cycles after the last electrical pulse delivered (see **Fig. 4a**). Acoustic stimuli consisted of a

646   distress (same syllable used for the passive listening experiments) and an echolocation call

647   (duration, 1.2 ms; spectrum shown in **Fig. 4b**), both presented at 50 dB SPL (rms). All

648   possible combinations of acoustic stimulus type (i.e. distress or echolocation) and sound onset

649   delay were pseudorandomly presented 25 times each. The interval between a trial block (i.e.

650   electric pulse train and acoustic stimulus) was of 2.5 seconds. Sounds were also presented

651   without any prior electrical stimulation ("no-Estim" condition), with a variable inter-stimulus

652   interval between 4 and 16 seconds, a total of 50 times each. Acoustic stimuli were delivered

653   using the same speaker setup described above, but for these experiments a different sound

654   card was used (RME Fireface UC; 16 bit precision, 192 kHz; RME Audio, Haimhausen,

655   Germany).

656   Comparisons of auditory cortical response strength between Estim and no-Estim conditions

657   were made by calculating the energy of the event-related potential (ERP). Specifically, the

658   response strength was calculated as the area under the curve of the absolute value of the

659   Hilbert-transform of the high-frequency component (25 – 80 Hz) of the ERP, for the first 150

660   ms after sound onset. We used the high frequency component of the ERP to avoid biases

661   related with low-frequency pre-stimulus trends in the LFPs. Because the number of trials

662   differed in the Estim and no-Estim conditions (i.e. 25 and 50, respectively), the response

663   strength of the no-Estim condition was calculated using 25 randomly selected trial out of 50.

664   The ERP is sensitive to the number of trials as it is a trial-average response; the number of

665   trials must therefore be equalized. Only then we compared response strengths between Estim

666   and no-Estim conditions, for each channel and delay relative to the last electrical pulse

667   delivered. Statistical comparisons were made with FDR-corrected Wilcoxon signed-rank tests,

668   with an alpha of 0.05. The effect sizes of these comparisons were calculated using the Cliff's

669   delta metric (a non-parametric approach). Effect sizes are considered negligible when Cliff's

670   delta < 0.147, small when $0.33 \leq$ Cliff's delta < 0.33, medium when $0.33 \leq$ Cliff's delta <

671   0.474, and large when Cliff's delta ≥ 0.474 [58]. On account of selecting 25 random trials from

672   the no-Estim condition, the above procedures were repeated 500 times, with the aims of

673   testing whether the outcomes of the statistical comparisons (Estim vs. no-Estim response

674   strength) were reliable and independent of the randomized trial selection.

675   Statistical procedures

676   All statistical analyses were made with custom-written MatLab scripts. Paired and unpaired

677   statistical comparisons were performed with Wilcoxon singed-rank and rank sum tests,

678   respectively. These are appropriately indicated in the text, together with sample sizes and p-

679   values. All statistics, unless otherwise noted, were corrected for multiple comparisons with

680   the False Discovery Rate approach, using the Benjamini and Hochberg procedure [86]. An alpha

681   of 0.05 was set as threshold for statistical significance. The effect size metric used, unless

682   stated otherwise (as in the GLM case), was Cohen's d:

683    $$d = \frac{\mu_{D1} - \mu_{D2}}{\sqrt{(\frac{(n_1-1)\sigma_{D1}^2 + (n_2-1)\sigma_{D2}^2}{n_1+n_2-2})}} \qquad [8],$$

684   where D1 and D2 are two distributions, μ represents the mean, σ^2 represents the variance,

685   while n_1 and n_2 are the sample sizes. Effect sizes were considered small when $|d| < 0.5$,

686   medium when $0.5 <= |d| <= 0.8$, and large when $|d| > 0.8$ [87].

687   To test differences in the connectivity graphs across conditions (e.g. echolocation vs.

688   communication, or passive listening vs. active vocalization), we obtained adjacency matrices

689   for each of the 500 penetrations (one per dPTE connectivity matrix; see above) and compared

690   the distributions using Wilcoxon signed rank tests. Given that the large sample size (n = 500

691   here) increases the occurrence of significant outcomes in statistical testing, edges were only

692   shown when comparisons were significant and produced large effect sizes ($|d| > 0.8$).

693   When comparing connectivity graphs between pre-voc and post-voc conditions, we used the

694   exact same trials per repetitions to construct the distribution of dPTE matrices for the pre- and

695   post-voc cases. A certain repetition *m* for each condition was then treated as paired, and

696   therefore Wilcoxon signed rank tests were used for comparing (as opposed to unpaired

697   statistics above). Again, only edges representing significant differences ($p_{corr} < 0.05$) with

698   large effect sizes were shown.

699   **Conflict of interests**

700   The authors declare no financial or non-financial conflicts of interest.

701   **Acknowledgments**

705

706   **References**

707   1.   Jurgens U. The neural control of vocalization in mammals: a review. *J Voice* **23**, 1-10 (2009).

708
709   2.   Okobi DE, Jr., Banerjee A, Matheson AMM, Phelps SM, Long MA. Motor cortical control of
710   vocal interaction in neotropical singing mice. *Science* **363**, 983-988 (2019).

711
712   3.   Zhang YS, Ghazanfar AA. A Hierarchy of Autonomous Systems for Vocal Production. *Trends
713   Neurosci* **43**, 115-126 (2020).

714
715   4.   Gavrilov N, Hage SR, Nieder A. Functional Specialization of the Primate Frontal Lobe during
716   Cognitive Control of Vocalizations. *Cell Rep* **21**, 2393-2406 (2017).

717

24

718   5.   Tschida K*, et al.* A Specialized Neural Circuit Gates Social Vocalizations in the Mouse. *Neuron*
719   **103**, 459-472 e454 (2019).

720
721   6.   Schulz GM, Varga M, Jeffires K, Ludlow CL, Braun AR. Functional neuroanatomy of human
722   vocalization: an H215O PET study. *Cereb Cortex* **15**, 1835-1847 (2005).

723
724   7.   Eliades SJ, Tsunada J. Auditory cortical activity drives feedback-dependent vocal control in
725   marmosets. *Nature Communications* **9**, (2018).

726
727   8.   Eliades SJ, Wang X. Neural substrates of vocalization feedback monitoring in primate auditory
728   cortex. *Nature* **453**, 1102-1106 (2008).

729
730   9.   Zhang S*, et al.* Organization of long-range inputs and outputs of frontal cortex for top-down
731   control. *Nat Neurosci* **19**, 1733-1742 (2016).

732
733   10.   Helfrich RF, Knight RT. Cognitive neurophysiology of the prefrontal cortex. *Handb Clin Neurol*
734   **163**, 35-59 (2019).

735
736   11.   Choi EY, Drayna GK, Badre D. Evidence for a Functional Hierarchy of Association Networks. *J
737   Cogn Neurosci* **30**, 722-736 (2018).

738
739   12.   Petkov CI, Jarvis ED. Birds, primates, and spoken language origins: behavioral phenotypes
740   and neurobiological substrates. *Front Evol Neurosci* **4**, 12 (2012).

741
742   13.   Voorn P, Vanderschuren LJ, Groenewegen HJ, Robbins TW, Pennartz CM. Putting a spin on
743   the dorsal-ventral divide of the striatum. *Trends Neurosci* **27**, 468-474 (2004).

744
745   14.   Hage SR, Nieder A. Single neurons in monkey prefrontal cortex encode volitional initiation of
746   vocalizations. *Nat Commun* **4**, 2409 (2013).

747
748   15.   Roy S, Zhao L, Wang X. Distinct Neural Activities in Premotor Cortex during Natural Vocal
749   Behaviors in a New World Primate, the Common Marmoset (Callithrix jacchus). *J Neurosci* **36**,
750   12168-12179 (2016).

751
752   16.   Weineck K, Garcia-Rosales F, Hechavarria JC. Neural oscillations in the fronto-striatal network
753   predict vocal output in bats. *PLoS Biol* **18**, e3000658 (2020).

754
755   17.   García-Rosales F, López-Jury L, González-Palomares E, Cabral-Calderín Y, Hechavarría JC.
756   Fronto-Temporal Coupling Dynamics During Spontaneous Activity and Auditory Processing in
757   the Bat Carollia perspicillata. *Frontiers in Systems Neuroscience* **14**, (2020).

758
759   18.   Park H, Ince RA, Schyns PG, Thut G, Gross J. Frontal top-down signals increase coupling of
760   auditory low-frequency oscillations to continuous speech in human listeners. *Curr Biol* **25**,
761   1649-1653 (2015).

762

763   19.   Plakke B, Romanski LM. Auditory connections and functions of prefrontal cortex. *Front*
764   *Neurosci-Switz* **8**, (2014).

765

766   20.   Kobler JB, Isbey SF, Casseday JH. Auditory pathways to the frontal cortex of the mustache
767   bat, Pteronotus parnellii. *Science* **236**, 824-826 (1987).

768

769   21.   Winkowski DE, Bandyopadhyay S, Shamma SA, Kanold PO. Frontal cortex activation causes
770   rapid plasticity of auditory cortical processing. *J Neurosci* **33**, 18134-18148 (2013).

771

772   22.   Winkowski DE*, et al.* Orbitofrontal Cortex Neurons Respond to Sound and Activate Primary
773   Auditory Cortex Neurons. *Cereb Cortex* **28**, 868-879 (2018).

774

775   23.   Martikainen MH, Kaneko K, Hari R. Suppressed responses to self-triggered sounds in the
776   human auditory cortex. *Cereb Cortex* **15**, 299-302 (2005).

777

778   24.   Aliu SO, Houde JF, Nagarajan SS. Motor-induced suppression of the auditory cortex. *J Cogn*
779   *Neurosci* **21**, 791-802 (2009).

780

781   25.   Rummell BP, Klee JL, Sigurdsson T. Attenuation of Responses to Self-Generated Sounds in
782   Auditory Cortical Neurons. *J Neurosci* **36**, 12010-12026 (2016).

783

784   26.   Baess P, Horvath J, Jacobsen T, Schroger E. Selective suppression of self-initiated sounds in an
785   auditory stream: An ERP study. *Psychophysiology* **48**, 1276-1283 (2011).

786

787   27.   Eliades SJ, Wang X. Sensory-motor interaction in the primate auditory cortex during self-
788   initiated vocalizations. *J Neurophysiol* **89**, 2194-2207 (2003).

789

790   28.   Flinker A, Chang EF, Kirsch HE, Barbaro NM, Crone NE, Knight RT. Single-trial speech
791   suppression of auditory cortex activity in humans. *J Neurosci* **30**, 16643-16650 (2010).

792

793   29.   Eliades SJ, Wang X. Dynamics of auditory-vocal interaction in monkey auditory cortex. *Cereb*
794   *Cortex* **15**, 1510-1523 (2005).

795

796   30.   Tsunada J, Eliades SJ. Dissociation of Unit Activity and Gamma Oscillations during
797   Vocalization in Primate Auditory Cortex. *J Neurosci* **40**, 4158-4171 (2020).

798

799   31.   Clayton KK*, et al.* Auditory Corticothalamic Neurons Are Recruited by Motor Preparatory
800   Inputs. *Curr Biol*, (2020).

801

802   32.   Li S, Zhu H, Tian X. Corollary Discharge Versus Efference Copy: Distinct Neural Signals in
803   Speech Preparation Differentially Modulate Auditory Responses. *Cereb Cortex* **30**, 5806-5820
804   (2020).

805

806   33.   Schneider DM, Mooney R. Motor-related signals in the auditory system for listening and
807   learning. *Curr Opin Neurobiol* **33**, 78-84 (2015).

808
809   34.   Toyomura A*, et al.* Neural correlates of auditory feedback control in human. *Neuroscience*
810   **146**, 499-503 (2007).

811
812   35.   Kingyon J*, et al.* High-gamma band fronto-temporal coherence as a measure of functional
813   connectivity in speech motor control. *Neuroscience* **305**, 15-25 (2015).

814
815   36.   Behroozmand R*, et al.* Sensory-motor networks involved in speech production and motor
816   control: an fMRI study. *Neuroimage* **109**, 418-428 (2015).

817
818   37.   Loh KK*, et al.* Cognitive control of orofacial motor and vocal responses in the ventrolateral
819   and dorsomedial human frontal cortex. *Proc Natl Acad Sci U S A* **117**, 4994-5005 (2020).

820
821   38.   Fernandez AA, Fasel N, Knörnschild M, Richner H. When bats are boxing: aggressive
822   behaviour and communication in male Seba's short-tailed fruit bat. *Anim Behav* **98**, 149-156
823   (2014).

824
825   39.   Knornschild M, Feifel M, Kalko EKV. Mother-offspring recognition in the bat Carollia
826   perspicillata. *Anim Behav* **86**, 941-948 (2013).

827
828   40.   Knornschild M, Feifel M, Kalko EKV. Male courtship displays and vocal communication in the
829   polygynous bat Carollia perspicillata. *Behaviour* **151**, 781-798 (2014).

830
831   41.   Hechavarria JC, Beetz MJ, Macias S, Kossl M. Distress vocalization sequences broadcasted by
832   bats carry redundant information. *J Comp Physiol A Neuroethol Sens Neural Behav Physiol*
833   **202**, 503-515 (2016).

834
835   42.   Fenzl T, Schuller G. Dissimilarities in the vocal control over communication and echolocation
836   calls in bats. *Behav Brain Res* **182**, 173-179 (2007).

837
838   43.   Gooler DM, O'Neill WE. Topographic representation of vocal frequency demonstrated by
839   microstimulation of anterior cingulate cortex in the echolocating bat, Pteronotus parnelli
840   parnelli. *J Comp Physiol A* **161**, 283-294 (1987).

841
842   44.   Buzsaki G, Anastassiou CA, Koch C. The origin of extracellular fields and currents--EEG, ECoG,
843   LFP and spikes. *Nat Rev Neurosci* **13**, 407-420 (2012).

844
845   45.   García-Rosales F, Beetz MJ, Cabral-Calderin Y, Kössl M, Hechavarria JC. Neuronal coding of
846   multiscale temporal features in communication sequences within the bat auditory cortex.
847   *Communications Biology* **1**, 200 (2018).

848
849   46.   Helfrich RF, Knight RT. Oscillatory Dynamics of Prefrontal Cognitive Control. *Trends Cogn Sci*
850   **20**, 916-930 (2016).

27

47. Lakatos P, Karmos G, Mehta AD, Ulbert I, Schroeder CE. Entrainment of neuronal oscillations as a mechanism of attentional selection. *Science* **320**, 110-113 (2008).

48. Lakatos P, Musacchia G, O'Connel MN, Falchier AY, Javitt DC, Schroeder CE. The Spectrotemporal Filter Mechanism of Auditory Selective Attention. *Neuron* **77**, 750-761 (2013).

49. Fries P. Rhythms for Cognition: Communication through Coherence. *Neuron* **88**, 220-235 (2015).

50. Eiermann A, Esser KH. Auditory responses from the frontal cortex in the short-tailed fruit bat Carollia perspicillata. *Neuroreport* **11**, 421-425 (2000).

51. Zhang W, Yartsev MM. Correlated Neural Activity across the Brains of Socially Interacting Bats. *Cell* **178**, 413-428 e422 (2019).

52. Rose MC, Styr B, Schmid TA, Elie JE, Yartsev MM. Cortical representation of group social communication in bats. *Science* **374**, eaba9584 (2021).

53. Franken MK, Eisner F, Acheson DJ, McQueen JM, Hagoort P, Schoffelen JM. Self-monitoring in the cerebral cortex: Neural responses to small pitch shifts in auditory feedback during speech production. *Neuroimage* **179**, 326-336 (2018).

54. Schmitt LM*, et al.* A neurophysiological model of speech production deficits in fragile X syndrome. *Brain Commun* **2**, (2020).

55. Hillebrand A*, et al.* Direction of information flow in large-scale resting-state networks is frequency-dependent. *Proc Natl Acad Sci U S A* **113**, 3867-3872 (2016).

56. Lobier M, Siebenhuhner F, Palva S, Palva JM. Phase transfer entropy: a novel phase-based measure for directed connectivity in networks coupled by oscillatory interactions. *Neuroimage* **85 Pt 2**, 853-872 (2014).

57. Ma J, Kanwal JS. Stimulation of the basal and central amygdala in the mustached bat triggers echolocation and agonistic vocalizations within multimodal output. *Front Physiol* **5**, 55 (2014).

58. Romano J, Kromrey JD, Coraggio J, Skowronek J. Appropriate statistics for ordinal level data: Should we really be using t-test and Cohen'sd for evaluating group differences on the NSSE and other surveys. In: *annual meeting of the Florida Association of Institutional Research* (ed^(eds) (2006).

59. Gilmartin MR, Balderston NL, Helmstetter FJ. Prefrontal cortical regulation of fear learning. *Trends Neurosci* **37**, 455-464 (2014).

28

896

897   60.   Forseth KJ, Hickok G, Rollo PS, Tandon N. Language prediction mechanisms in human
898   auditory cortex. *Nat Commun* **11**, 5240 (2020).

899

900   61.   Eliades SJ, Wang X. Comparison of auditory-vocal interactions across multiple types of
901   vocalizations in marmoset auditory cortex. *J Neurophysiol* **109**, 1638-1657 (2013).

902

903   62.   Nelson A, Schneider DM, Takatoh J, Sakurai K, Wang F, Mooney R. A circuit for motor cortical
904   modulation of auditory cortical activity. *J Neurosci* **33**, 14342-14353 (2013).

905

906   63.   Schneider DM, Nelson A, Mooney R. A synaptic and circuit basis for corollary discharge in the
907   auditory cortex. *Nature* **513**, 189-194 (2014).

908

909   64.   Abbasi O, Gross J. Beta-band oscillations play an essential role in motor-auditory interactions.
910   *Hum Brain Mapp* **41**, 656-665 (2020).

911

912   65.   Ford JM, Roach BJ, Faustman WO, Mathalon DH. Out-of-synch and out-of-sorts: dysfunction
913   of motor-sensory communication in schizophrenia. *Biol Psychiatry* **63**, 736-743 (2008).

914

915   66.   Miller CT, Thomas AW, Nummela SU, de la Mothe LA. Responses of primate frontal cortex
916   neurons during natural vocal communication. *J Neurophysiol* **114**, 1158-1171 (2015).

917

918   67.   Roy A, Svensson FP, Mazeh A, Kocsis B. Prefrontal-hippocampal coupling by theta rhythm and
919   by 2-5 Hz oscillation in the delta band: The role of the nucleus reuniens of the thalamus.
920   *Brain Struct Funct* **222**, 2819-2830 (2017).

921

922   68.   Sang N*, et al.* Human sensory cortex structure and top-down controlling brain network
923   determine individual differences in perceptual alternations. *Neurosci Lett* **636**, 113-119
924   (2017).

925

926   69.   Fox MD, Corbetta M, Snyder AZ, Vincent JL, Raichle ME. Spontaneous neuronal activity
927   distinguishes human dorsal and ventral attention systems. *Proc Natl Acad Sci U S A* **103**,
928   10046-10051 (2006).

929

930   70.   Simmons JA. Bats use a neuronally implemented computational acoustic model to form
931   sonar images. *Curr Opin Neurobiol* **22**, 311-319 (2012).

932

933   71.   Eliades SJ, Wang X. Neural correlates of the lombard effect in primate auditory cortex. *J
934   Neurosci* **32**, 10737-10748 (2012).

935

936   72.   Behroozmand R, Karvelis L, Liu H, Larson CR. Vocalization-induced enhancement of the
937   auditory cortex responsiveness during voice F0 feedback perturbation. *Clin Neurophysiol* **120**,
938   1303-1312 (2009).

939

940   73.   Esser KH, Eiermann A. Tonotopic organization and parcellation of auditory cortex in the FM-
941   bat Carollia perspicillata. *Eur J Neurosci* **11**, 3669-3682 (1999).

942
943   74.   Garcia-Rosales F*, et al.* Laminar specificity of oscillatory coherence in the auditory cortex.
944   *Brain Struct Funct* **224**, 2907-2924 (2019).

945
946   75.   Bokil H, Andrews P, Kulkarni JE, Mehta S, Mitra PP. Chronux: a platform for analyzing neural
947   signals. *Journal of neuroscience methods* **192**, 146-151 (2010).

948
949   76.   Zempeltzi MM*, et al.* Task rule and choice are reflected by layer-specific processing in rodent
950   auditory cortical microcircuits. *Commun Biol* **3**, 345 (2020).

951
952   77.   Nakagawa S, Schielzeth H. A general and simple method for obtaining R2 from generalized
953   linear mixed-effects models. *Methods Ecol Evol* **4**, 133-142 (2013).

954
955   78.   Lobier M, Palva JM, Palva S. High-alpha band synchronization across frontal, parietal and
956   visual cortex mediates behavioral and neuronal effects of visuospatial attention. *Neuroimage*
957   **165**, 222-237 (2018).

958
959   79.   Wibral M, Vicente R, Lindner M. Transfer Entropy in Neuroscience. In: *Directed Information*
960   *Measures in Neuroscience* (ed^(eds Wibral M, Vicente R, Lizier JT). Springer Berlin Heidelberg
961   (2014).

962
963   80.   Young CK, Ruan M, McNaughton N. A Critical Assessment of Directed Connectivity Estimates
964   with Artificially Imposed Causality in the Supramammillary-Septo-Hippocampal Circuit. *Front*
965   *Syst Neurosci* **11**, 72 (2017).

966
967   81.   Scott SK, Young AW, Calder AJ, Hellawell DJ, Aggleton JP, Johnson M. Impaired auditory
968   recognition of fear and anger following bilateral amygdala lesions. *Nature* **385**, 254-257
969   (1997).

970
971   82.   Tadel F, Baillet S, Mosher JC, Pantazis D, Leahy RM. Brainstorm: a user-friendly application
972   for MEG/EEG analysis. *Comput Intell Neurosci* **2011**, 879716 (2011).

973
974   83.   Atencio CA, Shih JY, Schreiner CE, Cheung SW. Primary auditory cortical responses to
975   electrical stimulation of the thalamus. *J Neurophysiol* **111**, 1077-1087 (2014).

976
977   84.   Yazdan-Shahmorad A*, et al.* Estimation of electrode location in a rat motor cortex by laminar
978   analysis of electrophysiology and intracortical electrical stimulation. *J Neural Eng* **8**, 046018
979   (2011).

980
981   85.   Takahashi S, Muramatsu S, Nishikawa J, Satoh K, Murakami S, Tateno T. Laminar responses in
982   the auditory cortex using a multielectrode array substrate for simultaneous stimulation and
983   recording. *Ieej T Electr Electr* **14**, 303-311 (2019).

984

985   86.   Benjamini Y, Hochberg Y. Controlling the False Discovery Rate - a Practical and Powerful
986   Approach to Multiple Testing. *J Roy Stat Soc B Met* **57**, 289-300 (1995).

987

988   87.   Cohen J. *Statistical power analysis for the behavioral sciences*, 2nd edn. L. Erlbaum Associates
989   (1988).

990

991

992

Figure legends

Fig. 1. Pre-vocal oscillations in frontal and auditory cortices predict ensuing vocal output. (**a**) Oscillograms (top) and spectrogram (bottom) of exemplary echolocation (left) and communication calls produced by *C. perspicillata*. (**b**) Cumulative probability distribution of echolocation (blue, n = 138) and communication (orange, n = 734) call lengths. No significance differences were observed (Wilcoxon rank sum test, p = 0.12). (**c**) (*Left*) Normalized average power spectral density (PSD) of echolocation (blue) and communication (orange) calls. (*Right*) Distribution of peak frequencies of echolocation and communication utterances; communication calls were significantly higher in frequency than their counterparts (p = 2.24×10^{-66}). (**d**) Single-trial LFPs recorded simultaneous to echolocation and communication utterances. The vertical red dashed line, at time 0, indicates the moment of vocalization onset. The top 16 traces correspond to LFPs recorded in the FAF; the bottom 16 LFP traces were recorded from the AC. Auditory cortical layers are marked. LFP amplitude was normalized within structure independently. (**e**) Average pre-vocal (-500 to 0 ms, relative to call onset) power spectral densities (PSD) at a representative depth (300 μm) in FAF and AC. Blue: echolocation; orange: communication; black, dashed: no-voc periods. The difference between echolocation and communication PSDs is depicted in grey (right). (**f**) Percentage pre-vocal power change across representative LFP bands (δ, 1-4 Hz; β_1, 12-20 Hz; γ_2, 60-120 Hz), relative to a no-voc baseline, across cortical depths in FAF (top) and AC (bottom). Values related to echolocation utterances (n = 138) are depicted in blue; those related to communication utterances (n = 734) are depicted in orange. Data shown as mean ± sem. (**g**) Pre-vocal power change in frontal and auditory regions predict vocalization type. Effect size (R^2_m) of GLMs considering all frequency bands and channels, both in frontal and auditory cortices. Effect sizes were considered small when $R^2_m < 0.1$, and medium for $R^2_m >= 0.1$. For illustrative purposes, effect size values from non-significant models were set to 0.

Fig. 2. Directed connectivity patterns in the FAF-AC network. (**a**) Graph visualization of directed connectivity between FAF and AC during no-voc periods. Channels in frontal and auditory cortices were combined into four categories: top (0-150 μm), mid1 (200-350 μm), mid2 (400-550 μm), and bottom (600-750 μm). Graph edges are weighted according to the strength of the preferred directionality (FAF→AC in blue; AC→FAF in orange; within area directionality in grey). Edges are only shown if there was significant preferred directionality according to a threshold defined by bootstrapping. (**b**) Similar to **a**, but directed connectivity was calculated in the pre-vocal echolocation and communication conditions. (**c**) Same as **b**, with connectivity patterns obtained for post-vocal echolocation and communication conditions.
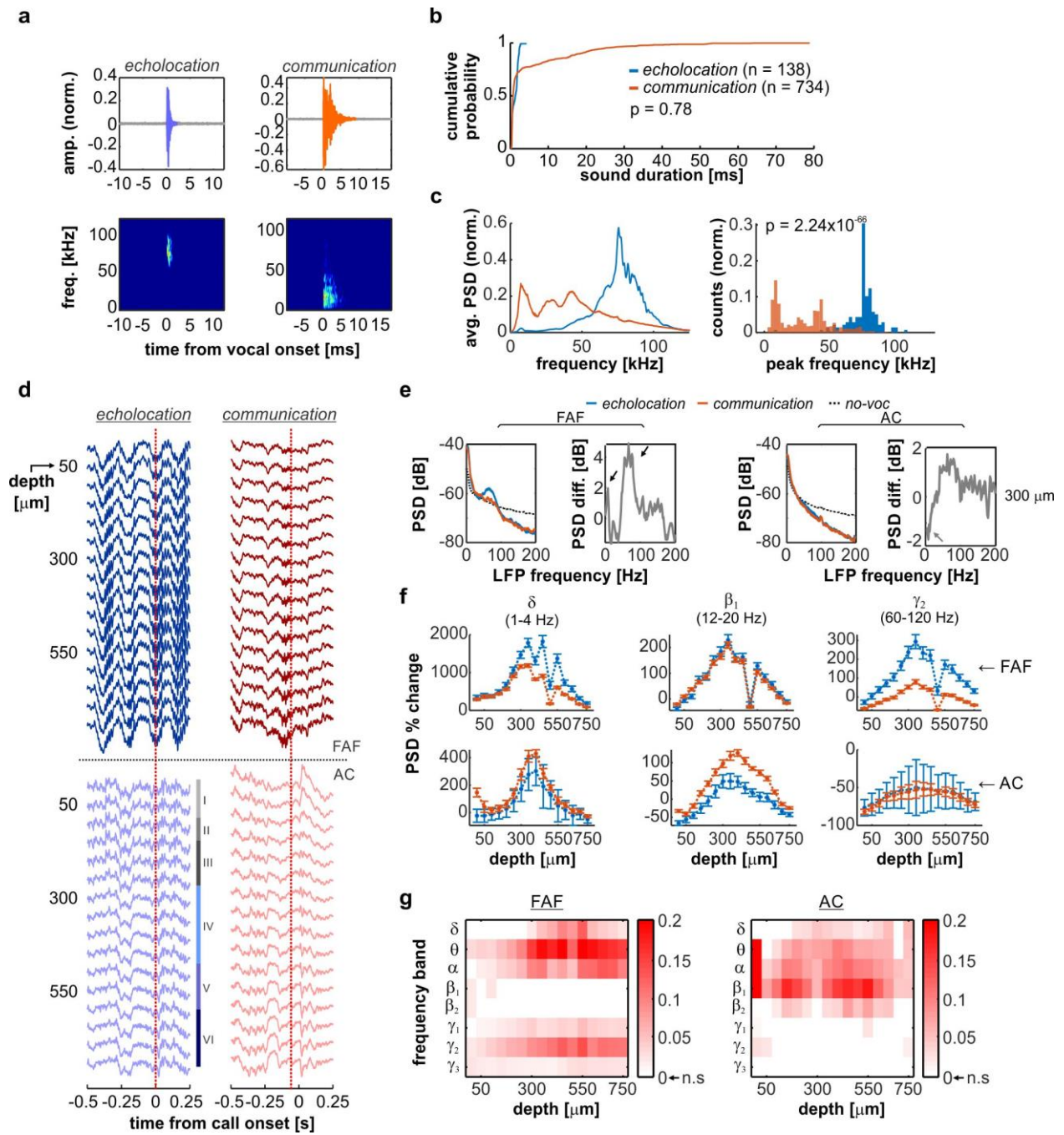
Fig. 3. Pre-vocal and post-vocal directionality differences in the FAF-AC network. (**a**) (*Top*) Graphs illustrating the differences between pre-vocal and post-vocal directionality, across frequency bands and during the production of echolocation calls. Edges were shown if three conditions were met: (i) the differences were significant (FDR-corrected Wilcoxon signed-rank tests, $p_{corr} < 0.05$), (ii) the effect size was large (|d| > 0.8), and (iii) edges were already significantly directional (see edges in **Fig. 2**). Edge thickness is weighted according to the effect size of the comparison. Continuous lines indicate pre-vocal dPTEs (first condition) higher than post-vocal dPTEs (second condition). Dashed lines indicate the opposite. (*Bottom*) Net information outflow (DI_{net}) from FAF (blue bars) and AC (orange bars), in the two conditions considered (pre-vocal vs. post-vocal). Significant differences across conditions are marked with stars (FDR-corrected Wilcoxon signed-rank tests; * $p_{corr} < 0.05$, ** $p_{corr} < 0.01$, *** $p_{corr} < 0.001$, n.s.: not significant; n = 500). Grey numbers in the panels indicate effect sizes (d; not shown for non-significant

1038   differences). Values were considered independently of whether there was previous significant
1039   directionality in any of the two conditions. Data shown as mean ± sem. (**b**) Same as in **a**, but
1040   illustrating comparisons of directionality between pre-vocal vs. post-vocal conditions related to the
1041   vocalization of communication calls.

1042   **Fig. 4. Electrical stimulation of the FAF increases response strength in AC.** (**a**) Schematic
1043   representation of the paradigm for electrical and acoustic stimulation. The timestamps for acoustic
1044   stimulation (coloured according to delay; see also panels **e**-**g**) represent the delay of sound onset
1045   relative to the end of electrical stimulation train. (**b**) Oscillograms of the natural distress syllable
1046   and echolocation pulse used for acoustic stimulation. On the right, the normalized power spectra of
1047   both calls are shown (orange, distress; blue, echolocation). (**c**) Broadband (0 – 10kHz), raw data
1048   recorded simultaneously from FAF and AC (at representative depths of 50, 250 and 600 μm)
1049   illustrating a single trial of electrical stimulation. Note that no electrical artefacts are visible in AC.
1050   (**d**) Auditory cortical LFPs (left column), and time-course of their energy (right), in response to
1051   either the distress syllable (top) or the echolocation pulse (bottom). Responses corresponding to the
1052   no-Estim conditions shown in blue; responses related to the Estim condition, in red. (**e**) Strength of
1053   auditory cortical ERPs in response to the distress syllable, across all recorded columns (n = 20) and
1054   depths. In blue, responses associated to the no-Estim condition; in red, those associated to the Estim
1055   condition (data as mean ± s.e.m). (**f**) Corrected p-values obtained after statistical comparisons
1056   between response strengths related to Estim and no-Estim conditions, across all channels and
1057   delays (paired, FDR-corrected Wilcoxon signed rank tests, alpha = 0.05). (**g-h**) Same as in **e-f**, but
1058   dealing with responses to the echolocation pulse. (**i**) Proportion iterations (out of 500) in which
1059   responses associated to the Estim condition were significantly larger than those associated to the
1060   no-Estim condition (same test as above). Data are presented across all channels and delays
1061   analysed, for responses to the distress and echolocation sounds. (**j**) Median effect size (Cliff's delta)
1062   for the same comparisons summarized in **i**.

1063   **Fig. 5. The FAF-AC network during vocal production.** (**a**) Oscillations in frontal and auditory
1064   cortices provide a neural correlate of vocal production, allowing the prediction of ensuing call type.
1065   Prediction is possible in complementary frequency bands in each region, and with opposite effects.
1066   (**b**) Schematic representation of causal interactions (within a TE framework) in the FAF-AC
1067   network. Strong top-down control, mostly in δ and γ frequencies, occurs during spontaneous
1068   activity (no-voc) and prior to vocal utterance. In the δ-band, information flows top-down in the
1069   circuit (FAF → AC) during pre-vocal periods, but changes to bottom-up (AC → FAF) information
1070   transfer during post-vocal periods. The directionality patterns and the strength of preferential causal
1071   interactions depend on the type of call produced, and on the timing relative to vocal onset. (**c**)
1072   Electrical stimulation results provide strong support to the notion that FAF alters the manner in
1073   which AC processes acoustic information, preferentially when animals listen to echolocation
1074   sounds. In comparison to listening of distress sounds, auditory cortical responses to echolocation
1075   sounds were more reliably enhanced after electrically stimulating the frontal cortex.
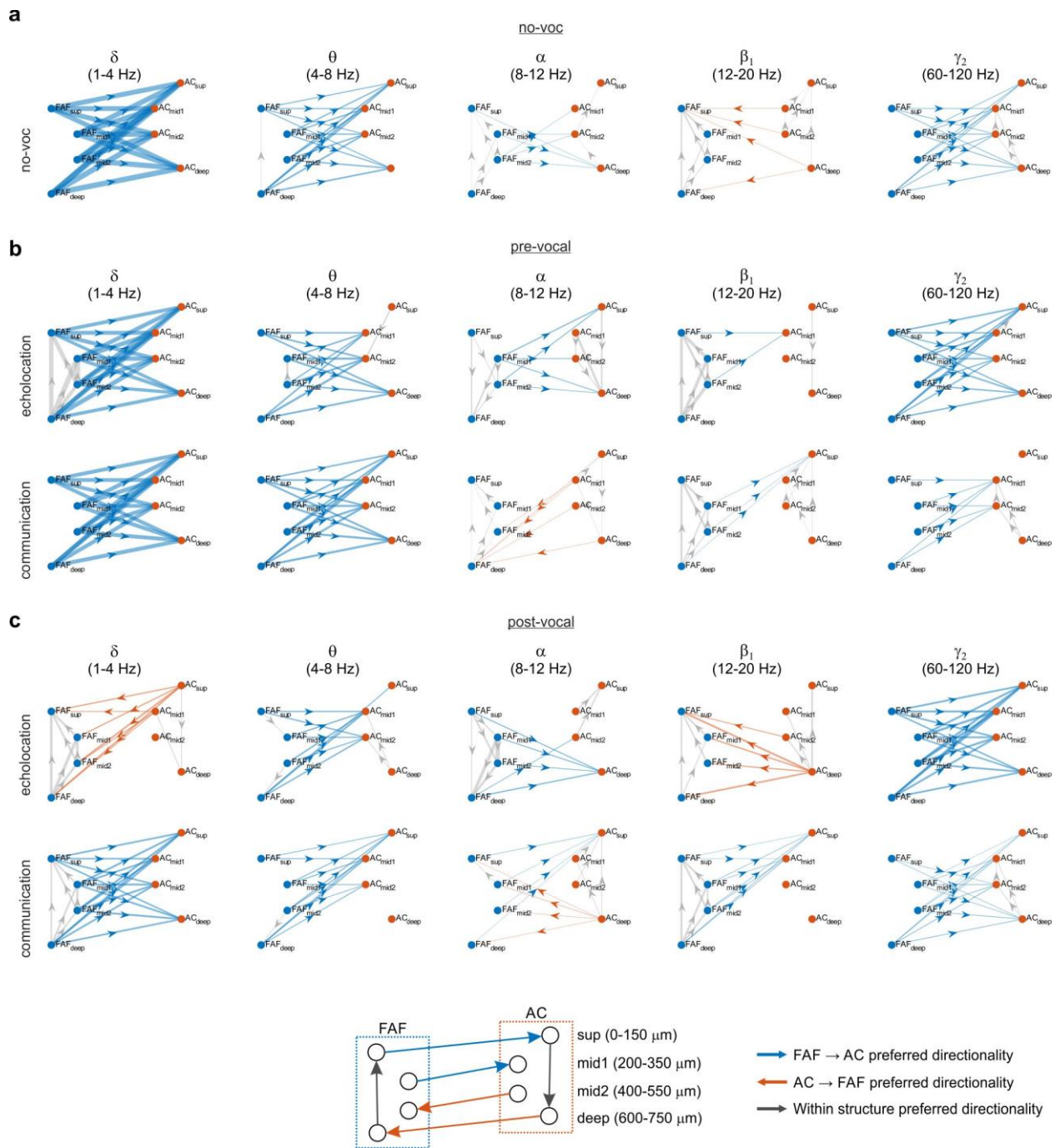
1076

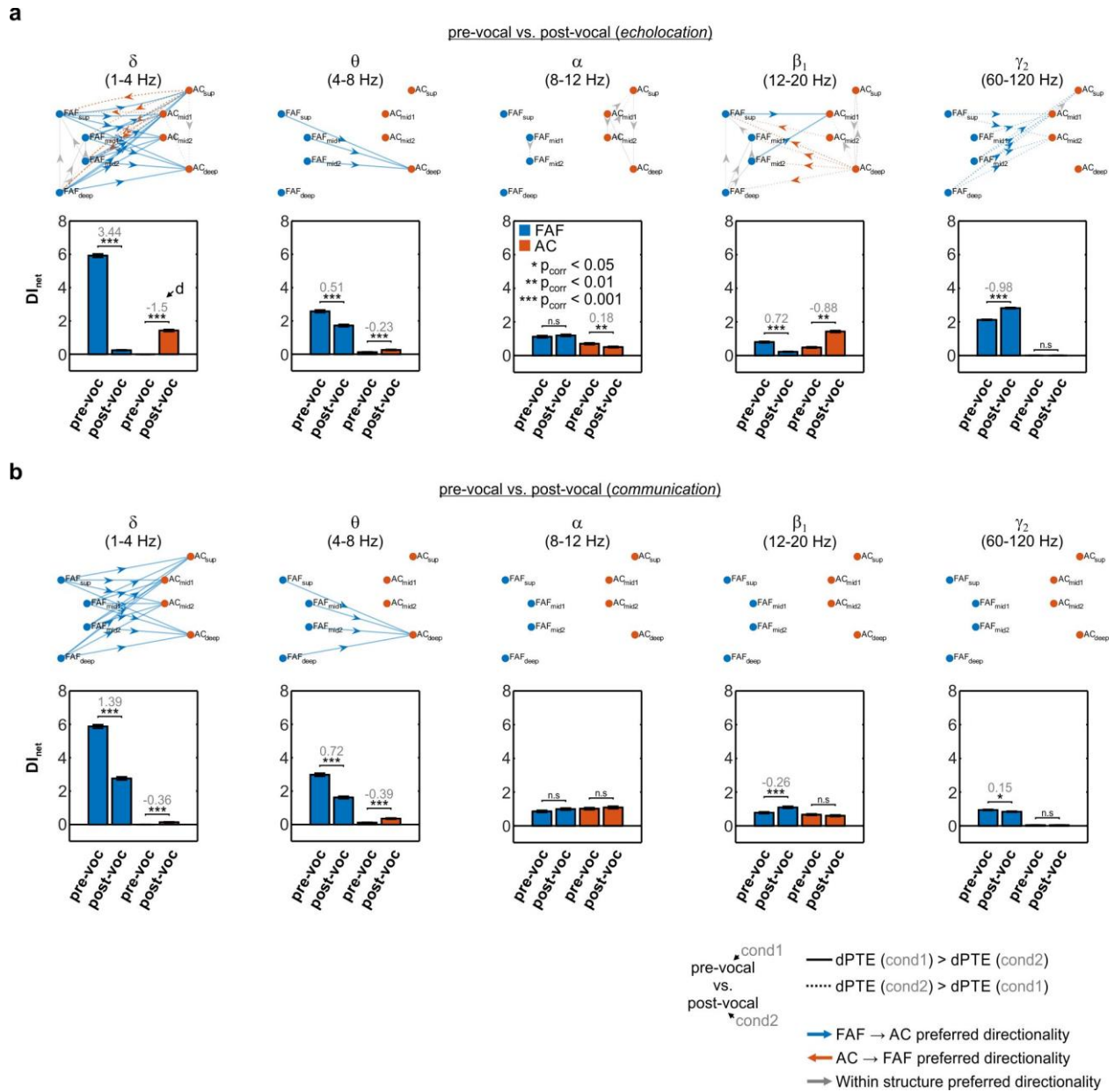**Fig. 1. Pre-vocal oscillations in frontal and auditory cortices predict ensuing vocal output.**

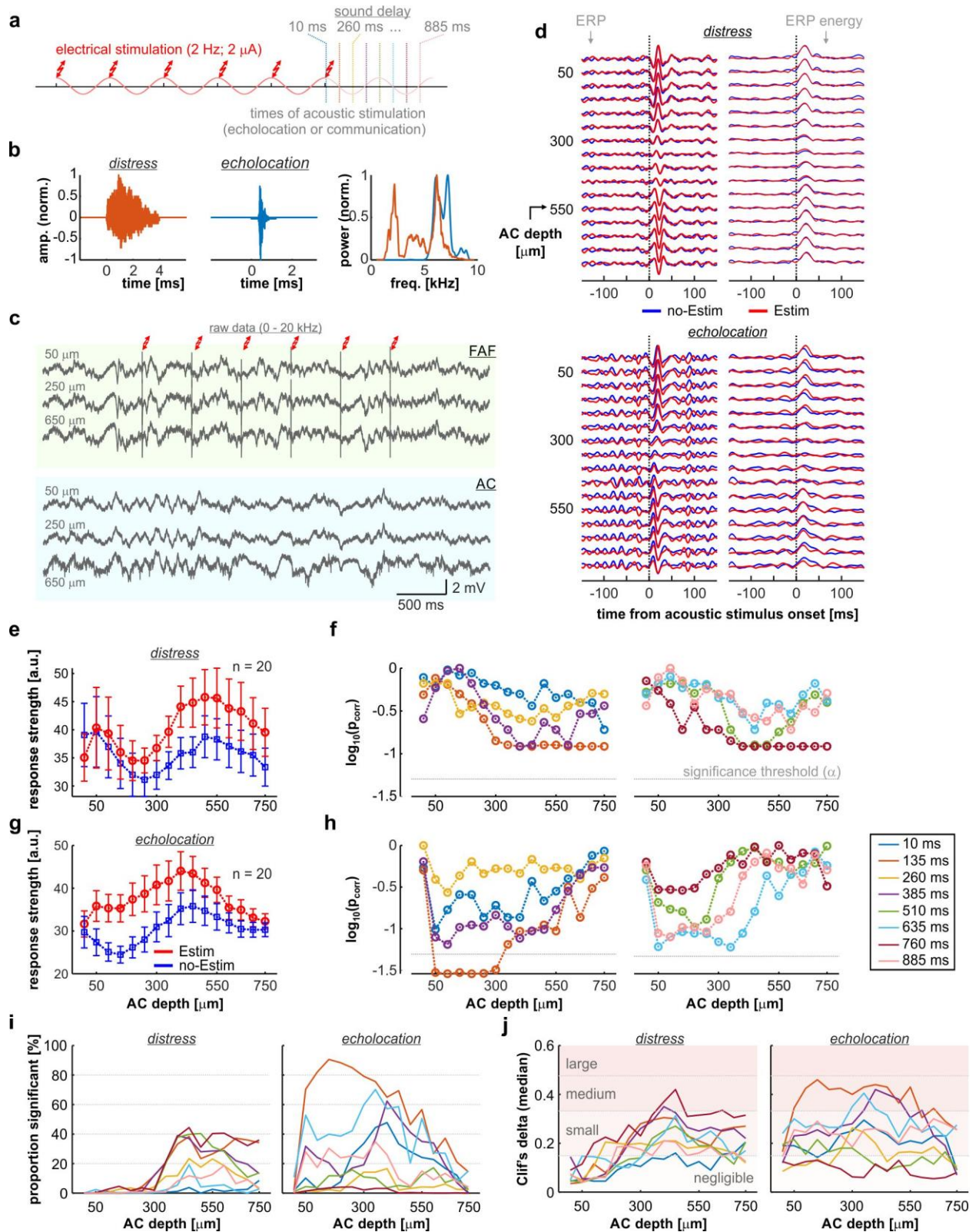**Fig. 2. Directed connectivity patterns in the FAF-AC network.**

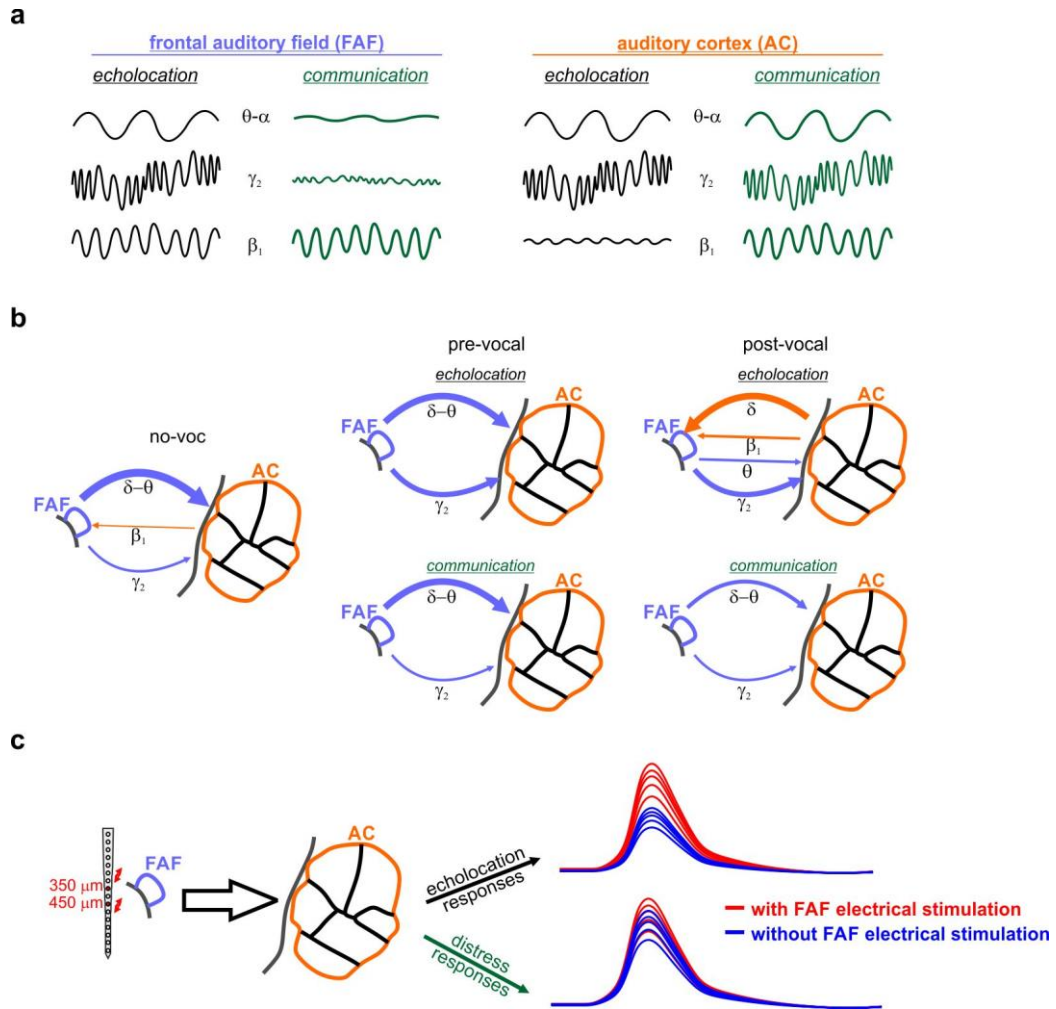**Fig. 3. Pre-vocal and post-vocal directionality differences in the FAF-AC network.**

Fig. 4. Electrical stimulation of the FAF increases response strength in AC.

1089

Fig. 5. The FAF-AC network during vocal production.

1091